# Silica-based fibers with axially aligned mesopores from chitin self-assembly and sol-gel chemistry

Bruno Alonso, Nathalie Witczak, Cyril Vallicari, Bastien Lecourt-Capdeville, Mathis Guiraud, Laurent Vachoud, Krassimir Kostov, Stefan Spirk, Gregor Trimmel, Emmanuel Belamie

# Silica-based fibers with axially aligned mesopores from chitin self-assembly and sol-gel chemistry

Bruno Alonso,[a]* Nathalie Witczak,[a] Cyril Vallicari,[a] Bastien Lecourt-Capdeville,[a] Mathis Guiraud,[a] Laurent Vachoud,[b] Krassimir L. Kostov,[c] Stefan Spirk,[d] Gregor Trimmel,[e] Emmanuel Belamie[a,f]*

[a] ICGM, Univ. Montpellier, CNRS, ENSCM, Montpellier, France

[b] Univ. Montpellier, UFR Sci Pharmaceut & Biol, UMR QualiSud, 15 av. Charles Flahault, BP14491, F-34093, Montpellier 5, France

[c] Institute of General and Inorganic Chemistry, Bulgarian Academy of Sciences, 1113 Sofia, Bulgaria.

[d] Institute of Bioproducts and Paper Technology, Graz University of Technology, Stremayrgasse 9, 8010 Graz, Austria

[e] Institute for Chemistry and Technology of Materials, NAWI Graz, Graz University of Technology, Stremayrgasse 9, 8010 Graz, Austria

[f] Ecole Pratique des Hautes Etudes, PSL Research University, 75014 Paris, France.

Corresponding authors: bruno.alonso@enscm.fr, emmanuel.belamie@enscm.fr

## Abstract

Polysaccharide nanorods (chitin, cellulose) can be used as colloidal templates to form silica-based mesoporous materials by combining self-assembly and sol-gel chemistry. Chitin nanorods are chosen here for their self-assembly properties, facile preparation from natural resources, and because of the complexing properties of the free amino groups at their surface in view of further functionalization. Electrospinning of ethanolic co-suspensions, containing the chitin nanorods as pore templates, siloxane oligomers as silica precursors and polyvinylpyrrolidone (PVP) as spinning polymer, allows for forming mats of hybrid organic-inorganic fibers with diameters in the 200-300 nm range. The relative proportions of each component can be adjusted to meet specific characteristics (e.g. micro-/mesoporosity ratio). After calcination, the fibers present an open porosity studied by TEM and $N_2$ volumetry. Elongated mesopores (100-200 nm long, 2-4 nm wide) are created by individual chitin monocrystals forming the nanorods. They are highly oriented along the fibers' axes with orientational order parameters $P_2 > 0.95$ for volume chitin contents $\phi_{chitin}^* \geq 0.2$. Additional microporosity is provided by the removal of the spinning polymer, PVP. Complementary viscosity measurements on the initial co-suspensions allow discussing the interactions between colloids and their possible impact on the materials' textures observed. The introduction of a monomeric $Ti^{4+}$ precursor in the co-suspensions leads to isolated and tetrahedral Ti units, distributed in the calcined porous silica fibers and possibly close to the pores surface. In addition, preliminary investigations on processing the fibers with a Zn xanthate as ZnS precursor leads to carbonized fibers with nanoparticles and a Zn/S molar ratio close to 1.

## Keywords

Chitin Nanorods, Electrospinning, Fibers, Self-assembly, Sol-Gel

## Highlights

- Hybrid organic-inorganic and porous silica-based fibers, several millimeters long and some hundreds of nanometers thick, have been synthesized through a simple one-pot approach that combines chitin nanorods' self-assembly, sol-gel chemistry and electrospinning.
- The chitin nanorods employed are bundles of monocrystals that are covered individually by silica during the process and form elongated mesopores after calcination.
- The mesopore texture is highly oriented along the fibers' axis (orientational order parameters $P_2 >$ 0.95). This high orientation is explained by a combination of the ability of the anisotropic chitin nanorods to assemble into mesophases, the shearing forces developed by the electrospinning process and the use of a long spinning polymer (PVP).
- From viscosity measurements of the initial co-suspensions, it is confirmed that PVP and chitin nanorods are strongly interacting favoring the high orientation of the texture.
- The electrospun porous silica fibers can be easily functionalized by incorporating specific precursors in the initial co-suspensions. This is demonstrated for the formation of porous silica fibers containing isolated and tetrahedral [$TiO_4$] units.

## Graphical abstract

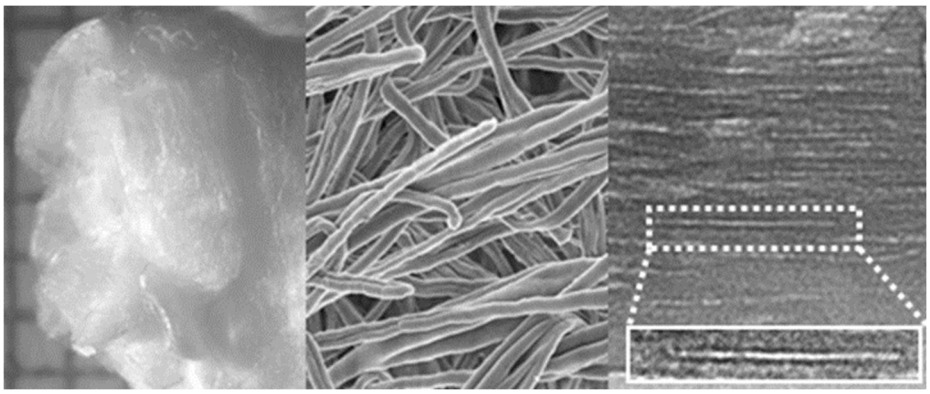

## 1. Introduction

Electrospinning has become a very popular method to produce fibers with diameters spanning from micrometers down to a few nanometers, and mature enough to consider production at the industrial scale [1,2]. The resulting mats obtained by the accumulation of fibers on a surface, expose nanostructured features and high surface area with a wide range of possible applications, from membranes, supported catalysis, solar and fuel cells, sensors to biomaterials such as tissue engineering [3,4].

In addition to the chemical composition, the control of the external and internal organization of the fibers forming the mats is of paramount importance for applications. For instance, alignment of electrospun fibers can be achieved by applying an external mechanical, electric or magnetic field to impart anisotropy to the resulting materials [2], with the aim of improving for instance mechanical [5] or electrical [6] properties. Uniaxial alignment can also be sought for biomedical applications of electrospun materials where cell alignment is favorable, for instance for vascular tissue engineering [7,8] or to favor nerve regeneration [9,10]. Besides the disposition of the fibers forming the mat, orientational order in the internal structure of the fibers also strongly determines their properties [11-13]. The long polymer chains often used to produce electrospun fibers have a strong tendency to align during processing with the flow direction due to strong shear forces, sometimes combined with additional external fields [14]. Nanoparticles can also be dispersed within the electrospun fibers[2,15] to improve their mechanical properties [5,16,17] or provide additional functionalities [12,18-23]. Anisotropic nanoparticles such as rods or platelets are often aligned along the long axis of the fiber due to shearing and interactions with the spinning polymer [17,19,20,24]. Additionally, applying an external magnetic field can allow fiber alignment [25], and particle alignment inside the fibers like for instance with Ag nanowires in association with PVP [22]. Conversely, the presence of nanoparticles was also shown to enhance the alignment of the POE polymer chains in the composite fibers due to confinement effects [26].

Self-supported membranes made of porous electrospun nanofibers exhibit internal porous surface area in addition to their external surface, thus providing improved surface-to-volume ratio and extended solid-air or solid-liquid interfaces. This is particularly needed when adsorption of molecules at the materials' surface is required for trapping, detection or catalyzing chemical reactions. Several strategies have been employed to generate porous fibers [27-29], such as phase separation [30,31] and hard templating with $SiO_2$ nanoparticles followed by etching in HF to obtain flexible mats of porous carbon nanofibers with improved electrochemical properties [32]. Sol-gel processes have also been widely used to form porous inorganic materials. After the first report on electrospun sol-gel $TiO_2$ nanofibers [33], several approaches have been described to generate extra porosity, often using sacrificial organic components for electrospinning typically removed by high temperature calcination [29]. The incorporation of amphiphilic molecules, following the principles of the evaporation induced self-assembly (EISA) approach [34], successfully led to electrospun mesoporous titania fibers exhibiting remarkable activity as photocatalyst or solid-state dye-sensitized solar cell [35-37]. In parallel, Choi *et*

*al*.[38] additionally suggested that the regular ordering and alignment of $TiO_2$ nanoparticles improved the photocatalytic performances. This effect can be attributed in part to enhanced transport in aligned nanostructures as suggested by several experimental [39,40] and modeling [41,42] works. Mesoporous fibers of other oxides like silica were also obtained with the EISA adapted approach [43,44]. Besides, it has been noticed that ordered mesostructures are difficult to achieve with this approach [45], and that only a careful tuning of the electrospinning and evaporation conditions allows to increase the degree of ordering [46].

In an effort towards greener and renewable synthesis routes, biopolymers have drawn great interest from the community to template inorganic materials, in particular using the relatively gentle physical conditions (temperature, pressure, pH) of sol-gel chemistry. In this context, a wide range of processing methods have been investigated with electrospinning being a particularly promising one [47,48]. In recent years, interactions between polysaccharide nanorods coming from the biomass (chitin, cellulose) and precursors of inorganic phases have been studied and used to form new hybrid organic-inorganic and mesoporous materials. In particular, the self-assembly properties of cellulose or chitin whiskers were exploited to elaborate such hybrid or porous materials exhibiting textures reminiscent of the nanorods liquid crystalline organization [49-65]. Different approaches have been used for that purpose such as the replication of polysaccharide nanorods liquid crystals [49,60], the formation of polysaccharide nanorods decorated with specific inorganic moieties or the colloidal co-assembly of polysaccharide nanorods and inorganic or organometallic precursors stabilized in hybrid suspensions [55,66,67]. This latter approach bears several advantages among which the shaping of the materials using sol-gel processes. In this context, microparticles and thin films have been elaborated using spray-drying and spin-coating respectively [66,68]. Another advantage is the possible orientation of the nanorods' assembly during the sol-gel transition using external fields. When ethanolic co-suspensions containing chitin nanorods and siloxane oligomers are subjected to slow solvent evaporation inside a static magnetic field, it becomes possible to align the diamagnetic nanorods, and further their mesoporous imprints, over several millimeters [66]. Besides, positively charged chitin nanorods in water suspensions can be aligned using alternating electric fields [69], and this behavior was transferred to chitin nanorods in the ethanolic co-suspensions so as to form textures with aligned pores [70], The colloidal co-assembly approach is also able to tune the composition of the inorganic phase in order to synthesize functional materials with optimized properties as shown for mesoporous silica-titania microspheres acting as efficient catalysts for the mild oxidation of bulky sulfur compounds [71,72].

The aim of this work was to combine these advantages of the colloidal co-assembly approach to synthesize silica-based mesoporous fibers with oriented textures, that can be functionalized for desired applications. The choice of chitin nanorods as polysaccharide template brings opportunities for fibers' functionalization thanks to the complexing properties of the free amino groups at their surface in addition to hydroxyl groups. For the sol-gel processing, we have chosen to start with a lab electrospinning setup known to form non-woven mats of micrometric or sub-micrometrics fibers. The

present developments of the electrospinning process, may allow in the future to elaborate aligned fibers using rotating electrodes or composite fibers using co-axial spinning, or to produce large quantities of fibers using larger experimental setups. In this article, we describe the morphology and texture of the produced materials. We study the effects of varying the composition of the co-suspensions, including a linear polymer for better spinning, and we try to decipher the interactions between the reactants by analyzing the rheological behavior of the initial suspensions, and the variations in pore texture (type and orientation) of the final fibers. First results on fibers' functionalization with isolated tetrahedral Ti units and ZnS particles are also presented.

## 2. Experimental

### 2.1 Synthesis and preparation of precursors´ suspensions

Chitin powder (60 mesh) extracted from shrimp shells was kindly provided by France Chitin. Aqueous suspensions of $\alpha$-chitin nanorods ($L$ = 260 ± 80 nm and $D$ = 23 ± 3 nm, as previously determined by TEM) were prepared following a procedure described elsewhere [73], based on the hydrolysis of chitin in boiling HCl (4 M) for 120 min. These nanorods are composed of several elongated chitin monocrystals ($D$ = 3.6 ± 0.6 nm as measured by cryo-TEM) [66]. The nanorods preparation involves elimination of excess HCl by dialysis, followed by ultrasound dispersion prior to the purification by low- and high-speed centrifugation cycles. Under these conditions, the percentage of deacetylation was estimated to be ~25 % (by conductivity and IR measurements). The suspensions concentration was set between approx. 1 to 3 wt% depending on the final targeted compositions for electrospinning. Stable dispersions in ethanol were obtained after ultrasound treatment and solvent exchange with pure ethanol.

An alcoholic solution containing siloxane oligomers (3 $mmol.g^{-1}$) was obtained by mixing under reflux (4 h) TEOS (ABCR, purity > 99.9%) and $10^{-1}$ M aqueous HCl in absolute ethanol (Sigma-Aldrich, purity > 99.8%) with the molar composition 1 TEOS: 2 $H_2O$: 2 EtOH. These conditions allowed for the initiation of hydrolysis and condensation reactions until a global equilibrium is reached upon refluxing. The resulting siloxane oligomers have an average hydrodynamic diameter of $D_h$ = 2.9 ± 0.2 nm (by dynamic light scattering) and an average degree of siloxane condensation of 0.72 ± 0.01 (from $^{29}Si$ liquid-state NMR) [67].

Preliminary tests showed that addition of a polymer to the colloidal suspension was required to form fibers by electrospinning. We used polyvinylpyrrolidone (PVP, Alfa Aesar) with a high molecular weight of Mw = 1,300,000 $g.mol^{-1}$, first dried in an oven (12 hours at 60° C and 1 hour at 100 °C), then weighed and dissolved in ethanol at an initial concentration of ca. 10 w%. Prior electrospinning, the final PVP concentrations $C_{PVP}$ are in the range 3 to 4 wt%.

In what follows, we describe the composition of the co-suspensions using the final PVP concentration $C_{PVP}$ and the volume fractions of the chitin $\phi_{chitin}$ and sol-gel silica $\phi_{silica}$ present in the hybrid materials after ethanol evaporation. Volume fraction are estimated from:

$\phi_{chitin} = V_{chitin} / \Sigma V$

$\phi_{silica} = V_{silica} / \Sigma V$

$\phi_{PVP} = V_{PVP} / \Sigma V$

with $\Sigma V = V_{chitin} + V_{silica} + V_{PVP}$ , $V_X$ corresponding the volume of the compound/phase $X$ in the as-synthesized fibers.

For comparison with previous works on chitin-silica nano-composites, we also used a reduced chitin volume fraction parameter $\phi_{chitin}$*:

$\phi_{chitin}^* = V_{chitin} / (V_{chitin} + V_{silica})$

The densities employed for volume calculations were 1.425, 1.90, and 1.2 g.cm$^{-3}$ for chitin,[74]sol-gel silica xerogels [75] and PVP [76], and 4.0 g.cm$^{-3}$ for $TiO_2$ and ZnS components.

In the preparation of suspensions for the electrospinning of silica fibers, the siloxane oligomers suspension was first mixed with the PVP solution and stirred until a homogeneous mixture was obtained. The chitin suspension was then added dropwise under stirring.

*Suspensions for silica-titania fibers:* $Ti^{4+}$ containing silica mesoporous fibers were simply obtained by mixing together the sol of siloxane oligomers and titanium(IV) bis(acetylacetonate) diisopropoxide (Aldrich, 75 wt% in $^{i}$PrOH) before adding the other reactants (PVP, and then chitin nanorods). The molar proportion of Ti relative to Si was fixed to $n_{Ti}/(n_{Ti} + n_{Si}) = 0.33$. Other parameters are $\phi_{PVP} = 0.66$ and $\phi_{chitin} = 0.16$ ($\phi_{chitin}^* = 0.46$). All the other processing parameters were identical to those of silica fibers.

*Suspensions for Zn xanthate functionnalization:* In order to achieve the most homogeneous suspensions, the protocol of suspension's formation has been slightly adapted. Zinc(II) O-2,2-dimethylbutyl dithiocarbonate (zinc xanthate) (synthesized according to reference [77]) (between 0.0 and 0.3 g) was solubilized in ethanol (20 mL). The solution was then mixed with the sol of siloxane oligomers and the chitin nanorods' suspension in ethanol. The intermediate suspension formed was subjected to rotary evaporation before addition of the PVP suspension. The PVP concentration before electrospinning $C_{PVP}$ was set in the 3-4 wt% range, and the final suspension was stirred until complete visual homogenization. The molar proportion of Zn relative to Si to $n_{Zn}/(n_{Zn} + n_{Si})$ was varied from 0 to 1 (values: 0.00, 0.05, 0.10, 0.25, 0.50 and 1.00). Other parameters were $\phi_{PVP} = 0.71$ and $\phi_{chitin} = 0.13$ ($\phi_{chitin}^* = 0.45$). All the other processing parameters were identical to those of silica fibers.

**2.2 Fibers' formation**

Mats of fibers were obtained by electrospinning using a lab scale apparatus (EC-ANL from IME technologies). The setup presents a flat copper electrode disk (5 cm in diameter) fitted with a metallic

needle in its center for the suspension to flow, and above a copper counter-electrode disk (5 cm in diameter) for the collection of fibers. Several optimization runs allowed us to find the range of processing conditions leading to well-defined fibers. The distance between electrodes was in the 20-25 cm range, the potential difference was set with a voltage of 20-25 kV, the ethanolic suspensions were delivered with a syringe pump at a flow rate of 15-30 µL/min. The relative humidity and the temperature were regulated to 40 ±10 % and 20 ±5 °C respectively. Several electrospinning runs were accumulated until the total amount of matter suited for application and analysis was reached, typically between 0.1 and 0.3 g. The collected organic-inorganic hybrid fibers were dried and stored in closed vessels at ambient temperature.

Calcining in air at 550°C during 8H lead to silica and silica-titania porous fibers.

For three zinc xanthate functionalized fibers ($n_{Zn}/(n_{Zn} + n_{Si}) = 0.06$, 0.10 and 0.24), post-treatments after fiber formation consisted in heating the samples under $N_2$ at 473 K for 1 H (xanthate decomposition) and then 1073 K for 1 H (carbonization).

**2.3 Characterization**

Thermogravimetric analyses (TGA) were conducted on a Perkin Elmer STA 6000 apparatus under air by heating the hybrid fibers at 10 K/min from 300 to 1173 K. EDX spectroscopy was performed by analyzing back-scattered electrons (5 independent measurements) with a SEM FEI Quanta 200F operated at 15 kV under low vacuum (0.3 Torr). Zn and S contents were determined by ICP-AES (Thermofisher apparatus, AETE-ISO platform, Montpellier, France) after mineralization ($HNO_3$ and HF acid route).

*NMR spectroscopy*

$^{29}$Si liquid-state NMR spectra were recorded on a Bruker 400 spectrometer, using 5 mm quartz tubes in $CDCl_3$, single $\pi/2$ ($^{29}$Si) pulses, $^1$H decoupling during acquisition, and 2.7 s of inter-pulse delay. $Cr(acac)_3$ was added before acquisition to insure a short longitudinal relaxation. $^{29}$Si solid-state NMR spectra were recorded on a Agilent-Varian 400 spectrometer ($\nu(^{29}Si) \equiv 79.5$ MHz), using 7.5 mm zirconia rotors ($\nu_{MAS} = 4$ kHz). Single $\pi/6$ ($^{29}$Si) pulses were used with $^1$H decoupling (RF field strength ~50 kHz) during acquisition and 60 s of recycling delays, insuring proper $^{29}$Si longitudinal relaxation. The siloxane condensation degree (or extent of condensation) was calculated using a weighted average $c = \Sigma(n.\%Q^n/400)$ where $\%Q^n$ is the signal area percentage of each $Q^n$ silica units connected to $n$ other silica units. Signal area percentages were obtained by spectrum fitting using the freely available *Dmfit* software [78][79].

*SEM*

Scanning Electron Microscopy (SEM) images were recorded using a Hitachi S-4500 I SEM. Fibres width was determined using Fiji software [80] from over 200 measurements per condition.

*TEM*

Transmission Electron Microscopy (TEM) analyses were made on a JEOL 1200 EX2 microscope operating at 100 kV. Calcined samples were embedded in a resin and sectioned into slices ~70 nm thick with an ultramicrotome (Reichert Leica Ultracut S). The TEM images were used to determine the dimensions of the clear areas, corresponding to pores coming formed after chitin calcination (see Results and discussion). They were also used to study the orientation of the elongated pores inside the fibers. For that purpose, between 80 to 290 measurements were done for each fiber composition. The orientational parameters $P_{2,x}$ are described in the Results and discussion section and in the supporting information SI6.

*XPS*

X-ray photoelectron spectroscopy (XPS) measurements were carried out on an AXIS Supra electron spectrometer (Kratos Analyical Ltd.) with base vacuum in the analysis chamber in the order of $10^{-8}$ Pa. The samples are irradiated with monochromatized Al $K_\alpha$ photons with energy of 1486.6 eV. The photoemitted electrons were separated, according to their kinetic energy, by a 180° -hemispherical analyzer with a total instrumental resolution of 0.6 eV (as measured by the FWHM of Ag $3d_{5/2}$ line) at pass energy of 20 eV. Due to charging effect a resolution of ~1.0 eV has been measured on the isolated samples. The analysis area was 700×300 $\mu m^2$. The concentrations (in at.%) of the observed chemical elements were calculated by normalizing the areas of their most intense photoelectron peaks to their relative sensitivity factors using the commercial software of the spectrometer. The experimental precision is ±0.1 eV.

*N2*

Nitrogen sorption isotherms were recorded using a Micrometrics Tristar apparatus at 77 K. Calcined samples were outgased at 523 K at $3 \cdot 10^{-3}$ Torr for at least 8 H. The pore volume fractions $\phi_{POR}$ were estimated using the maximum adsorbed volume of nitrogen sorption isotherms considering a density of 2.2 g $cm^{-1}$ for calcined silica. Specific surface areas ($S_{BET}$) were calculated using the BET method.[81] Average pore diameters $d_{p,BdB}$ were inferred from the nitrogen desorption branch using the correlation of Broekhoff and de Boer (BdB) [82], and considering the $p/p_0$ value at the inflexion point [83]. To inspect microporosity formation, *t*-plot analyses [84] have been undertaken using the equation of Harkins and Jura [85]. From the surfaces of multimolecular layers, we estimate the micropores' specific surface area and an approximate volume. Mesopores' specific surface area and volume are obtained by subtracting the micropores' values to $S_{BET}$ and pore volume.

*Rheology*

The rheological behavior of the suspensions were investigated with a rotational rheometer (Physica MCR 301, Anton-Paar) coupled with the Rheoplus software (v3.40) which recorded the data and allowed subsequent analysis. A cone/plate geometry (diameter: 5 cm, angle: 1°, truncation: 104 µm) was used as the measurement device. The cone/plate geometry was enclosed into a hermetic chamber saturated with ethanol vapor to prevent ethanol evaporation from the suspensions. The temperature was maintained constant at 25 ± 0.1 °C by a Peltier module. The rheological properties were investigated through flow measurements which consisted in imposing an increasing logarithmic ramp of shear rate to the sample (from 10 $s^{-1}$ to 5000 $s^{-1}$). Samples were not pre-sheared prior to rheological experiment and all measurements were performed in triplicate. The error on the measurement was about 10%. Experimental results were analyzed through the representation of the apparent viscosity $\mu$ as a function of shear rate $\dot{\gamma}$. The apparent viscosity $\mu$ (Pa.s) was defined as the ratio between the shear stress ( $\tau$, Pa) and the shear rate ($\dot{\gamma}$, $s^{-1}$).

## 3. Results and discussion

Fiber mats are synthesized by electrospinning ethanolic co-suspensions containing calibrated chitin nanorods ($L$ = 260 ± 80 nm, $D$ = 23 ± 3 nm), siloxane oligomers ($D_h$ = 2.9 ± 0.2 nm), and long PVP chains (Mw = 1 300 000 $g.mol^{-1}$) (**Fig. 1**). During the process, ethanol is evaporated and the hybrid organic-inorganic fibers are collected at the counter-electrode Their content in organic matter checked by TGA and their Si/N molar ratio checked by EDX are consistent as expected with that of the initial co-suspensions (**Fig. S1**). It is interesting to note that the Si/N ratio determined by XPS (**Fig. S1B**), that is sensitive to the uppermost surface layers of the fibers ($l \approx 2$ nm), is always significantly higher. Therefore the surface has a higher proportion in siloxane network than the whole fibers. This observation can be explained by the preferential positioning of the siloxane network around the chitin nanorods as observed in previous works on spray-dried chitin-silica microparticles [66]. The hybrid fibers are further transformed into porous silica fibers by calcination in air. Along these processes, the siloxane condensation degree $c$ estimated from $^{29}$Si NMR increases gradually. For a series of fibers with $\phi_{chitin}^*$ = 0.29, $c$ = 0.72 in the co-suspensions, $c$ = 0.84 in the hybrid fibers and $c$ = 0.92 in the calcined fibers (**Fig. S2**). Both hybrid and calcined fibers are in the form of self-standing mats (**Fig. 1**) possessing an intrinsic and macroscopic elasticity.

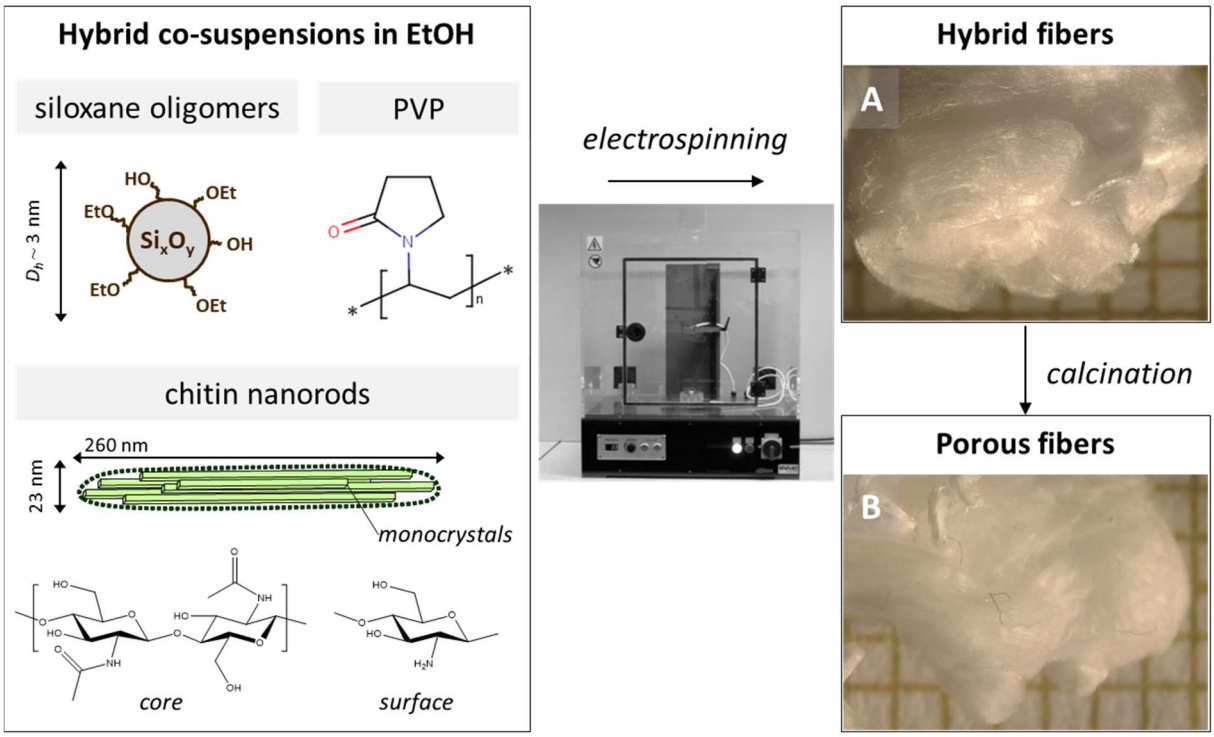


**Fig. 1.** Schematic description of the fibers formation through electrospinning. Pictures of electrospun fibers mats, before (A) and after calcination (B). The squares' sides in the pictures are 5 mm long.

### 3.1 Fiber characterization

*3.1.1 Scanning Electron Microscopy*

Typical morphologies of both hybrid and calcined fibers are presented in **Fig. 2**. These fibers have a roughly circular cross-section and a length well above the millimeter range (optical microscopy, **Fig. 1** and **Fig. S3**). The fibers diameter varies in the 0.2-1.0 µm range. With the compositions of the samples depicted in **Fig. 2**, the average hybrid fibers width $w_{ave}$ is typically 250 nm (see actual values indicated on each picture). Larger fibers were observed in some conditions, which actually corresponded to flat ribbons. The morphology depends on the initial composition of the co-suspensions and processing conditions. In some cases, we additionally noticed the formation of defects such as beads, which are commonly reported with electrospun materials [2]. However, as illustrated in **Fig. S4**, respective chitin and siloxane compositions could be varied with a fixed volume fraction of PVP ($\phi_{PVP}$ = 0.55 in **Fig. S4**), without noticeable changes in fibers morphology.

The overall fiber morphology is maintained after calcination (**Fig. 2B**, **2D**), although fractures along the fibers mains axis result in a decrease in length to some micrometers or tens of micrometers. The lateral dimensions of the fibers also appear slightly decreased upon calcination, e.g. by 18 % for $\phi_{chitin}$ = 0.1 and 26 % for $\phi_{chitin}$ = 0.3 (at constant $\phi_{PVP}$ = 0.55), as inferred from measurements on SEM images (**Fig. 2**). However, calcination does not compromise the mechanical strength of the fiber mats, provided enough matter has been deposited for fibers entanglements to impart cohesiveness to the materials (**Fig. 1**).

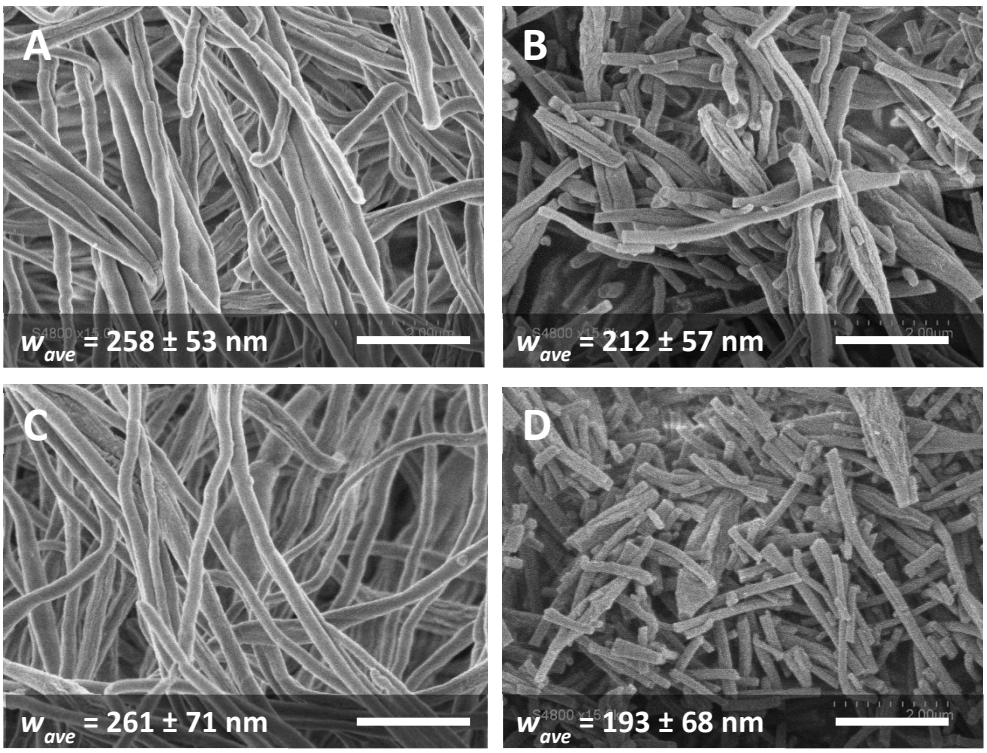


**Fig. 2.** SEM pictures of fibers with $\phi_{chitin}$* = 0.1 (A,B) and 0.3 (C,D) at a constant $\phi_{PVP}$ = 0.55, before (A,C) and after (B,D) calcination. The scale bars are 2 µm. The values at the bottom left of the images are the average fibers width $w_{ave}$ ± standard deviation.

*3.1.2 Transmission Electron Microscopy and nanorods' orientation*

The ultrathin sections of the calcined fiber mats have been observed by TEM (**Fig. 3**). The clear and elongated areas have diameters ($D$ = 2.0 ±0.8 nm) close to that of the initial chitin monocrystals ($D$ = 3.6 ±0.6 nm) forming the nanorods, which stands at the limit between micro- and meso-porosity [86]. They correspond to the porous imprints of chitin monocrystals after calcination in air, in agreement with previous works on bulk or spray-dried mesoporous silica obtained from chitin nanorods and siloxane oligomers co-assembly [66,87]. The smaller value of the pore diameters compared to the chitin monocrystal can be understood by a contraction due to siloxane condensation during the calcinations step or the preparation of the microtomed samples (solidification of the resin, compression by cutting), as well as to an underestimation of the diameters of tridimensional pores by TEM (artefacts or defocusing conditions) [88, 89]. Importantly, fibers produced in the same conditions with only PVP and siloxane oligomers, in the absence of chitin nanorods, do not exhibit these elongated porous imprints.

In situations where calcined fibers are cut transversally, i.e. along their main axis, strong uniaxial alignment of elongated pores is clearly visible, over the whole width and length of the fibers (**Fig. 3**). From a statistical analysis made on fibers with different initial compositions (**Fig. S5**), we have calculated the orientational parameters $P_2(\cos\theta) = (3.\langle\cos^2\theta\rangle - 1)/2$ where $\theta$ stands for the angle between elongated pores' main axes ($P_{2,inter}$) or the angle between the fibers' surface and the elongated pores'

main axis ($P_{2,surface}$). From the high values of these order parameters (0.86-0.99) presented in **Table 1**, we can state that the elongated pores are aligned between them and parallel to the fibers' surface. Further, we have estimated the distributions of angle deviations between the fibers' surface and the main axis of the elongated pores. Full width half maximum (FWHM) comprised between 5 and 22° are obtained from Gaussian fits of these distributions. These FWHM values are translated into a third orientational order parameter $P_{2,distribution}$ that takes into account the effect of angle distribution (**Table S1**) [90]. The values of $P_{2,distribution}$ are very close to that of the two other order parameters $P_2$ (**Table 1**). These fibers present therefore a highly oriented pore texture.

As seen above, we can consider that these elongated pores correspond to the imprints of chitin mono-crystals after calcination. The strong alignment and orientation of the elongated pores is therefore explained by the alignment of the chitin nanorods under the shearing force developed during electrospinning [15,20,24,91]. Shearing can affect directly the chitin nanoparticles possessing a relatively high aspect ratio ($L/D \sim 10$), or indirectly through the disentanglement and elongation of the PVP chains during fibril formation. In addition, chitin nanorods are forming mesophases in concentrated aqueous acidic or ethanolic suspensions (above ca. 2.5 and 1.5 wt% respectively) [92] that can be further translated into pore textures by co-assembly with siloxane oligomers and sol-gel processing [66,87]. It is to note that the fibers made here with the lowest amount of chitin ($\phi_{chitin}^* = 0.1$) lead to the less oriented pore textures as deduced from our measurements ($P_2 < 0.95$). This chitin volume fraction respect the silica content is also leading to less ordered texture in spray-dried microparticles [87]. On the contrary, higher chitin contents favor the formation of ordered mesophases and textures in these microparticles, and also in the presently studied electrospun fibers ($P_2 > 0.95$).

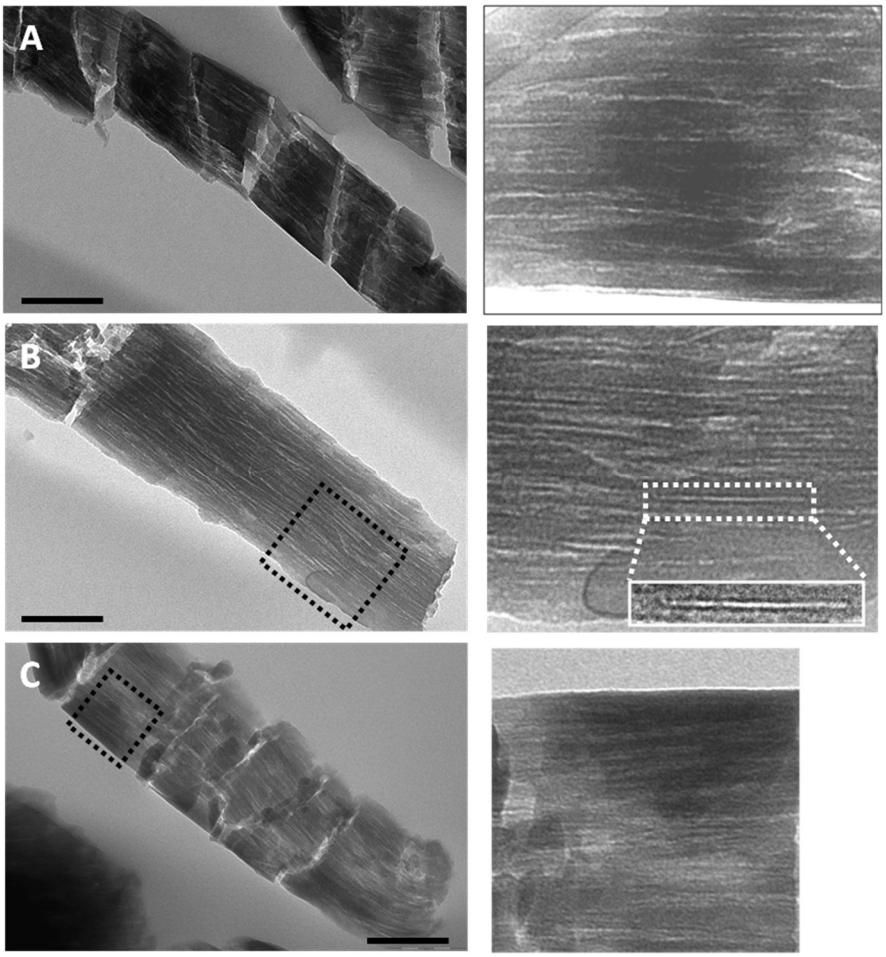


**Fig. 3.** TEM pictures of calcined fibers with $\phi_{chitin}$* = 0.13 (A), 0.16 (B) and 0.3 (C); $\phi_{PVP}$ = 0.55 (A) and 0.44 (B, C). The scale bars are 200 nm. Pictures on the right-hand side are enlargements to highlight chitin imprints alignment.

**Table 1.** Orientational order parameters from TEM measurements.

| $\varphi_{PVP}$ | $\varphi_{chitin}$* | $P_{2,inter}$ [a] | $P_{2,surface}$ [b] | $P_{2,distribution}$ [c] |
|---|---|---|---|---|
| 0.44 | 0.10 | 0.87 | 0.86 | 0.93-0.94 |
| 0.44 | 0.20 | 0.99 | 0.97 | 0.98-1.00 |
| 0.44 | 0.30 | 0.98 | 0.98 | 0.97-0.99 |
| 0.44 | 0.29 | 0.98 | 0.98 | 0.99 |
| 0.55 | 0.29 | 0.97 | 0.98 | 0.96-1.00 |

[a] Order parameter $(3\langle\cos^2\theta\rangle - 1)/2$ calculated for angles between mesopores' main axes inside the fibers. [b] Order parameter $(3\langle\cos^2\theta\rangle - 1)/2$ calculated for angles between the fibers' surface and the mesopores' main axis. [c] Order parameter that takes into account the distribution in angles between the fibers' surface and the mesopores' main axis (see **Table S1**).

*3.1.3 $N_2$ volumetry of calcined fibers*

Typical $N_2$ adsorption-desorption isotherms of calcined fibers are presented in **Fig. 4**. In the absence of chitin, the calcined fibers are mainly microporous. The presence of chitin nanorods in the electrospinning mixture leads to a type IV isotherm (**Fig. 4, curve B**) [86], characteristic of the capillary condensation occurring inside mesopores ($2 < d_p < 50$ nm) here with a $H_2$ type hysteresis loop. This kind of isotherm is very close to those measured for other mesoporous materials (bulk samples, microparticles) formed by our co-assembly approach [66,72,87]. In these previous studies, the shape of the hysteresis loop has been related to a wide pore size distribution originating from open and interconnected cavities of finite dimensions corresponding to the imprint of chitin mono-crystals, also in agreement here with TEM measurements (*vide supra*).

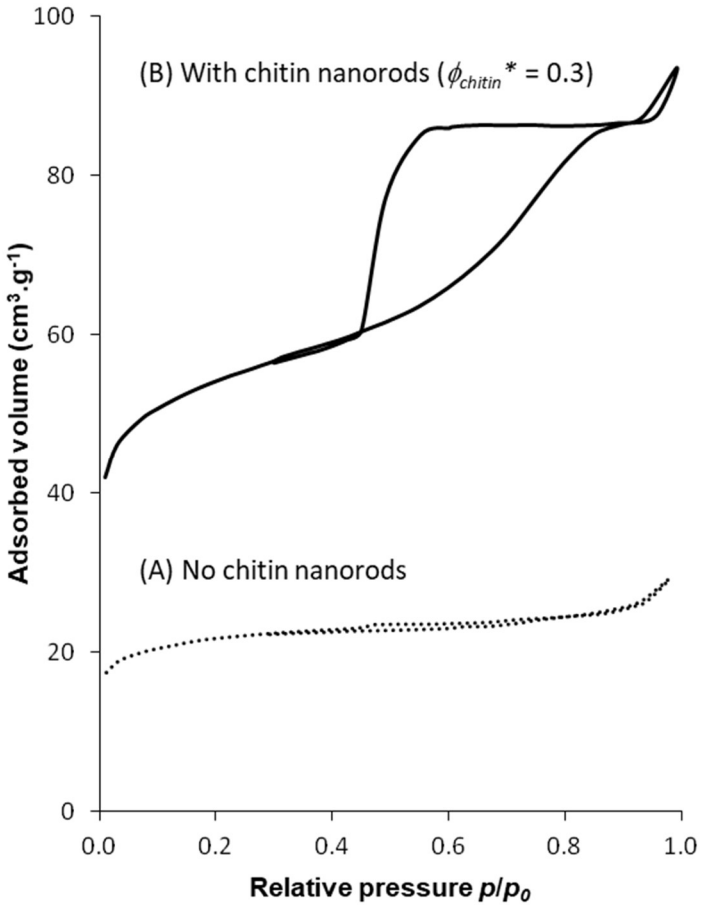


**Fig. 4**. Typical $N_2$ adsorption-desorption isotherms at 77K of calcined fibers ($\phi_{PVP}$ in hybrid fibers is 0.45). (A) Without chitin nanorods' addition. (B) With chitin nanorods ($\phi_{chitin}$* = 0.3).

As inferred from the isotherms' shapes (**Fig. 4**) and the correlation between the mesopore volume fraction $\phi_{mesopore}$ and $\phi_{chitin}$* ($r^2 \approx 0.86$, **Fig. 5**), the origin and the quantity of mesopores are clearly related to the chitin content. This was also demonstrated previously for the other mesoporous materials obtained

by the co-assembly of the same chitin source and siloxane colloids [66,87]. The mesopores thus result from the coating of the chitin mono-crystals by the siloxane network. It is also noteworthy that the initial PVP content can slightly affect $\phi_{mesopore}$ in particular for the highest content in chitin (**Fig. 5**).

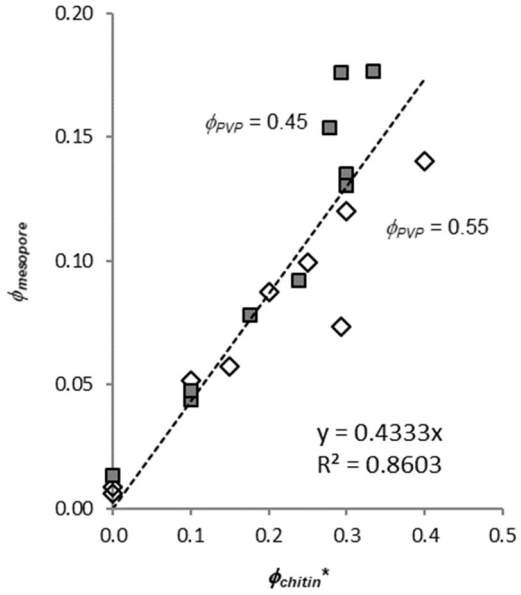


**Fig. 5.** Mesopore volume fraction $\phi_{mesopore}$ of calcined fibers as a function of reduced chitin volume fraction $\phi_{chitin}$* of the hybrid fibers. Filled squares (■) correspond to $\phi_{PVP}$ = 0.45 in the hybrid fibers, empty lozenges (◊) to $\phi_{PVP}$ = 0.55. Linear regression (dashed line) is for all samples, the corresponding fit equation and $R^2$ value are given on the graph.

In addition to mesoporosity, and in contrast to previous materials made by other co-assembly and sol-gel processing approaches, the electrospinning process and the concomitant use of PVP as a spinning polymer lead to a significant amount of microporosity in the calcined fibers. **Fig. 6** presents the correlations between specific surface area and pore volume for both micro- and mesoporosity. From the slope of the linear regressions and considering cylindrical pore morphology, we estimate rough values for the pore diameters: 1.9 nm for micropores and 4.2 nm for mesopores. This last value is consistent with the mesopore diameters (4.7-5.0 nm range) estimated from the desorption branch at the inflexion point of the hysteresis.

Interestingly, surface fractal dimensions calculated from $N_2$ sorption isotherms [93] are found to vary between 2.75-2.95 (highest values for samples with less chitin content), which indicates rather high surface roughness, higher than that measured for other mesoporous samples obtained by co-assembly and sol-gel routes [87]. This roughness of the pore walls might account to some extent for the discrepancy between the pore diameters estimated from TEM images and the larger values obtained by $N_2$ sorption data. In any case, the presence of a large hysteresis loop on the $N_2$ isotherms and of porous imprints in TEM only for samples prepared with chitin strongly support that the mesoporosity originates from the removal of the chitin during calcination.

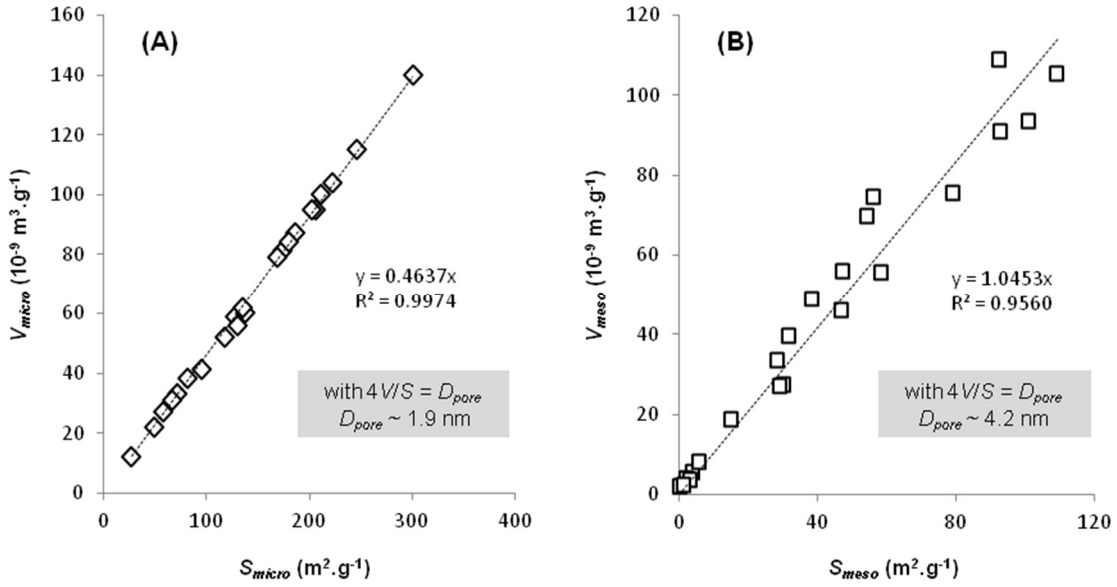


**Fig. 6.** Pore volume as a function of specific surface areas for: (A) micropores, (B) mesopores. All calcined fibers with different initial compositions are considered. PVP volume fractions $\phi_{PVP}$ are between 0.45 and 0.65, and reduced chitin volume fraction $\phi_{chitin}$* between 0.0 and 0.4. Pore diameters $D_{pore}$ are estimated from the slope ($y$ values) of linear regressions (dashed lines) considering cylindrical pore morphology.

Still, the presence of PVP and siloxane oligomers leads to microporous fibers (**Fig. 4A**), which suggests that the polymer added to promote fiber formation affects the final porosity in the calcined fibers through specific intermolecular interactions with chitin nanorods and siloxane oligomers.

### 3.2 Rheological study of the initial suspensions

TEM and $N_2$ volumetry studies suggest that PVP chains participate in the final materials texture, notably by promoting the orientation of chitin nanorods during processing, and also through specific intermolecular interactions with the two other colloids (chitin, siloxane). Besides, we have shown in previous works the existence of interactions between chitin or cellulose nanorods and siloxane oligomers favoring the formation of hybrid nano-composites [66,67]. Rheological studies of the initial suspensions can provide insights into the interactions between the colloidal reactants in the co-suspensions [92]. Under laminar flow, the apparent viscosity ($\mu$) corresponds to the resistance to the suspension flow and is related to the frictional forces and cohesion between fluid layers within the suspension. As a consequence, the viscosity is related to the interactions between the fluid layers, hence to the interactions between the components present in these fluid layers.

We have considered a co-suspension with a typical composition used in this work ($\phi_{chitin}$ * = 0.30, $\phi_{PVP}$ = 0.55, $C_{PVP}$ = 3 wt%). In **Fig. 7A**, we present the apparent viscosity plotted against shear frequency for this co-suspension, which is a quaternary mixture of chitin nanorods, PVP, siloxane oligomers and ethanol, and for suspensions containing only two components in ethanol (chitin + siloxane, chitin +

PVP, siloxane + PVP). In all cases, the concentration of each present component in ethanol is kept constant. As expected, the suspensions containing the long PVP chains are the most viscous ones. Furthermore, we notice that the highest apparent viscosity is obtained with mixtures of chitin nanorods and PVP chains, indicating the presence of an overall strong interaction between these colloids, possibly resulting from the various types of hydrogen bonds that can be formed (e.g. NH…O=C or OH…O=C), as well as van der Waals forces and excluded volume effects. However, the additional presence of siloxane oligomers significantly decreases the viscosity, indicating that siloxane-chitin and siloxane-PVP interactions hamper chitin-PVP interactions. Experimental curves are also compared to calculated ones obtained by summing the apparent viscosities of one-component suspensions (**Fig. 7B-E**). In **Fig. 7B**, the viscosity experimentally measured for the co-suspension containing chitin nanorods, siloxane oligomers and PVP chains is much higher than the calculated sum of viscosities measured for the three components alone (e.g. 69 and 23 $10^{-3}$ Pa.s respectively, at 9.9 $s^{-1}$). This again agrees well with the presence of strong interactions between colloids. In **Fig. 7C**, the difference between the viscosity of the chitin-PVP suspension and the sum of viscosities of chitin nanorods and PVP chains alone is even larger (e.g. 156 and 22 $10^{-3}$ Pa.s respectively, at 9.9 $s^{-1}$), confirming that the chitin nanorods-PVP chains interactions have the greatest effect on viscosity. We have seen previously that the interactions between siloxane oligomers and chitin nanorods can promote an increase in the viscosity of the suspensions after a threshold in siloxane oligomers concentration at a given chitin concentration [92]. Here, siloxane oligomers appear to have little effect on the viscosities of mixtures PVP+siloxane and chitin+siloxane at the concentration investigated (**Fig. 7D-E**). The threshold has not been reached in the case of chitin nanorods and siloxane suspensions, although the presence of siloxane oligomers at the same concentration strongly interferes in the colloidal interactions between PVP and chitin nanorods in the complete co-suspension.

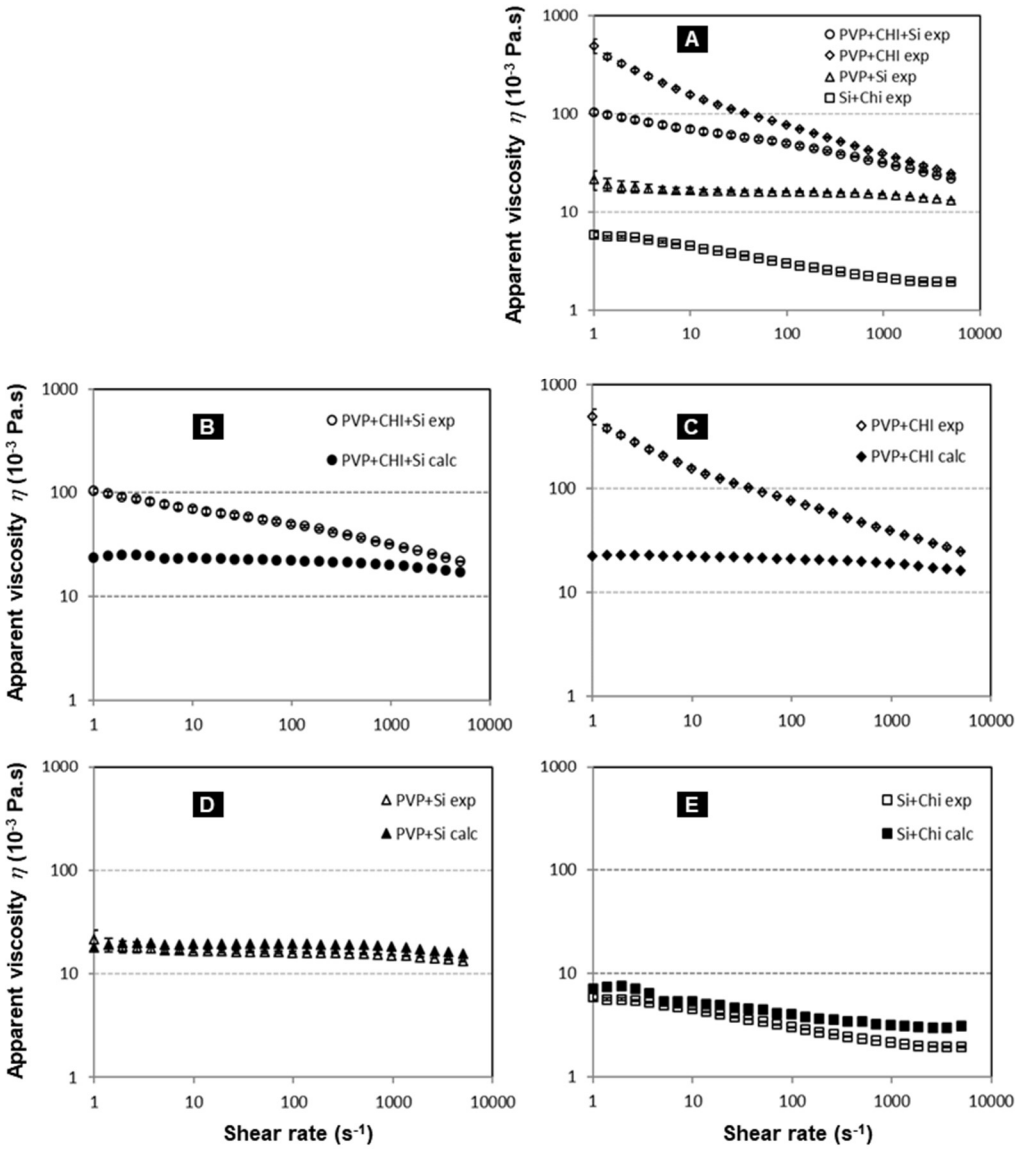


**Fig. 7.** Apparent viscosity as a function of shear rate for two- and three-component suspensions in ethanol, represented as the mean ± standard deviation (at least 3 measurements). The measured curves are named "exp" in the legend inserts. The calculated curves ("calc") were obtained by summing up the data, at each shear-rate value, measured for one-component suspensions (not shown). "Si" and "Chi" correspond to siloxane oligomers and chitin nanorods respectively. The composition of the three-component mixture in 7A is given by $\phi_{chitin}$ *= 0.30, $\phi_{PVP}$ = 0.55, $C_{PVP}$ = 3 wt%). In the other cases, the concentration of each component in ethanol is identical when present.

### 3.3 Fibers' functionalization

The porous silica fibers can be functionalized through the incorporation of other inorganic elements. For instance, electrospun mesoporous titania-silica fibers might present interesting catalytic properties. We previously demonstrated this was the case for titania-silica microparticles formed using the same colloidal co-assembly approach but with another sol-gel processing technique (spray-drying) [71,72]. Herein, we have successfully introduced $Ti^{4+}$ cations in the silica matrix by simply adding the monomer precursor $Ti(acac)_2(O^iPr)_2$ to the siloxane oligomers sol used in the co-suspensions. The morphology

(SEM) and texture (TEM, $N_2$ sorption isotherms) of the titania-silica fibers are very similar with or without titanium (**Fig. 8**). Besides, the initial Ti/Si molar ratio (calculated to be 0.50 in the suspension) is preserved after electrospinning and further calcination in air. It is estimated by EDX to be 0.50 in the hybrid fibers, and 0.48 in the calcined fibers. At the surface of the fibers (≈1-2 nm depth), this Ti/Si ratio is estimated by XPS to be 0.27 and 0.35 for hybrid and calcined fibers respectively. This difference in composition between the surface (as determined by XPS) and the core of the fibers is explained by a preferential interaction of the Ti precursor with the chitin nanorods' surface during the syntheses, possibly through a complexation by $–NH_2$ and –OH groups. After calcination, Ti atoms remain thus close to the chitin imprints forming the pores, and therefore at a distance from the fibers external surface probed by XPS. This observation is consistent with our previous conclusions on the related spray-dried microparticles [72]. In addition, for these calcined fibers, we found by XPS that about 97% of the Ti is forming $[TiO_4]$ tetrahedral $T_d$ units typical of dispersed $Ti^{4+}$ cations in silica, instead of $[TiO_6]$ octahedral $O_h$ units (≈3% here) of phase-separated titania (**Fig. S6-S7**). Both the high content in isolated $T_d$ units and the proximity of these units to the pore surface are promising properties for applications in catalysis using membranes of electrospun fibers, like those proven for spray-dried microparticles [71,72].

Last, we have started a preliminary study on hybrid fibers containing zinc xanthate precursors in view of the *in situ* formation of ZnS nanoparticles. Zinc xanthates are known to decompose under mild temperatures to yield metal sulfide nanocrystalline materials [94]. The synthesis protocol has been modified so as to spin homogeneous suspensions containing chitin nanorods, siloxane oligomers, zinc xanthate (in variable proportions relative to Si) and PVP (see Experimental section). Well-defined fiber mats were obtained, showing an evolution in fibers' morphology from cylindrical fibers towards flattened ribbons as the Zn content increases.(**Fig. S8**) The fibers lateral dimensions of some 100s of nanometers are consistent with those found without Zn xanthate functions. In the hybrid fibers, the relative contents in Zn estimated by EDX follow that of the initial suspensions (**Table S2**). Fibers' samples have been thermally treated to favor the formation of ZnS nanoparticles and carbonization (see Experimental section). Although the contrast in TEM pictures is smaller than for calcined fibers, it is possible to observe in the carbonized fibers elongated clear areas with the dimensions of chitin monocrystals and corresponding to chitin imprints or chitin carbonized crystals (**Fig. S9**). In addition, it worth mentioning that black spots of nanometer dimensions (1 to 10 nm in diameter) are observed on the fibers. Their size and observability increase with the Zn content. These spots are tentatively assigned to Zn based nanoparticles. In these carbonized fibers containing a majority of carbon and silica, the relative proportion of zinc decreases of about 40-50 % (EDX), possibly because of the high temperature used favoring Zn migration and evaporation. Besides, we studied more in detail the Zn/S molar ratio of one carbonized fibers' sample ($n_{Zn}/(n_{Zn} + n_{Si}) = 0.10$). Chemical analyses (ICP) and XPS analyses lead to Zn/S values of 1.0 and 1.2, in agreement with the expected formation of ZnS, while a value of 1.7 is obtained by EDX. The divergence can be explained by some heterogeneity in the sample that impacts more the EDX values obtained at each measurement (the error is estimated to 0.9 from standard

deviations). Although this is a preliminary study that would need a further investigation, in particular by the optimization of the carbonization process, it shows the possible extension of our method to the incorporation of very different functions in view of specific applications.

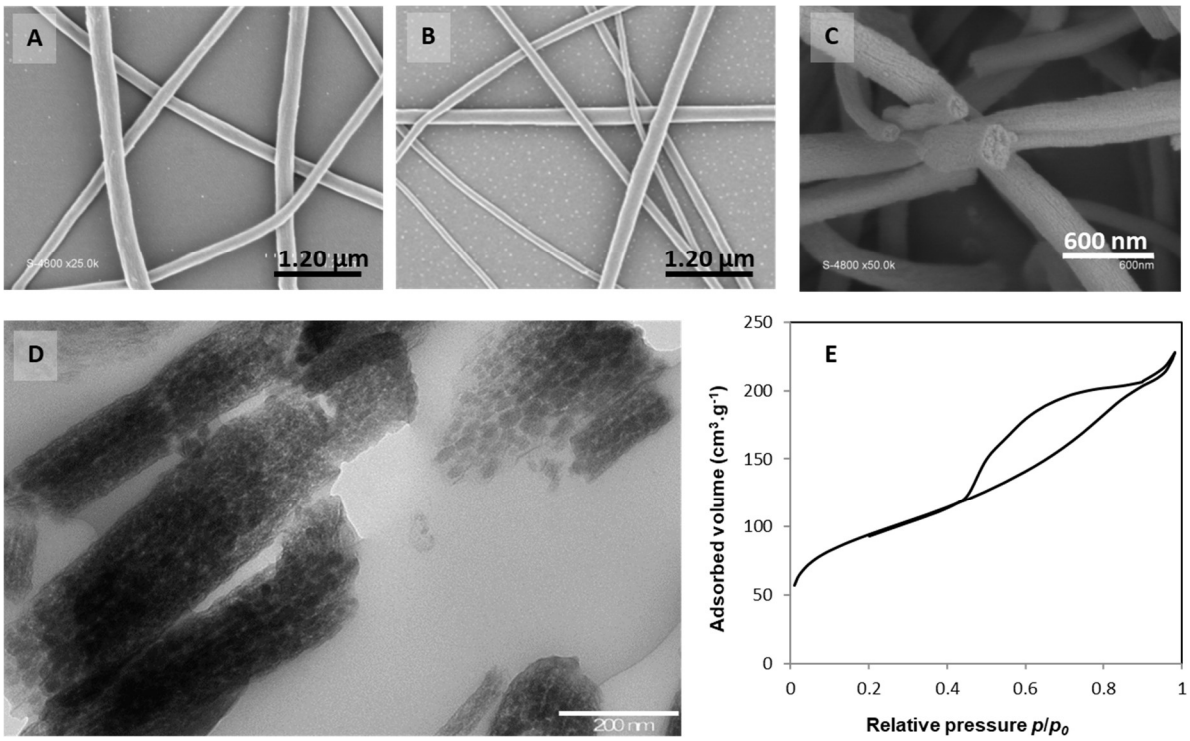


**Fig. 8.** Morphology and texture of titania-silica fibers. (A,B) SEM observation of fibers after electrospinning in the absence (A) ($\phi_{chitin}$ *= 0.53, $\phi_{PVP}$ = 0.68) or presence (B) of Ti precursor $Ti(acac)_2(O^iPr)_2$ ($\phi_{chitin}$*= 0.46, $\phi_{PVP}$ = 0.66) and Ti/Si = 0.5. (C) SEM observations of calcined Si-Ti fibers as in (B) and (D) observation of ultrathin sections of the same fibers in TEM. (E) shows a typical $N_2$ adsorption-desorption isotherms at 77 K of Si-Ti calcined fibers.

## 4. Conclusions

We have proposed a simple synthetic approach that combines self-assembly and sol-gel chemistry, and we have shown how ethanolic co-suspensions containing polysaccharide nanorods like chitin, siloxane oligomers and the spinning polymer PVP can form hybrid organic-inorganic electrospun fibers, several millimeters long and some hundreds of nanometers thick.

Calcination of the hybrid fibers leads to silica fibers possessing an open and porosity. The chitin nanorods are bundles of monocrystals that are covered individually by silica during the process and form elongated mesopores after calcination. The mesopore texture is highly oriented along the fibers' axis with orientational order parameters $P_2 > 0.95$ for significant volume chitin contents ($\phi_{chitin}* \geq 0.2$). This high orientation of the whole mesopore texture is explained by a combination of the ability of the anisotropic chitin nanorods to assemble into mesophases, the shearing forces developed by the electrospinning process and the use of a long spinning polymer (PVP). This latter polymer is

contributing to additional microporosity thanks to the existing interactions with siloxane oligomers. Interestingly, the relative proportions of each component (chitin, PVP, siloxane oligomers) can be adjusted to meet specific characteristics like the balance between micro- and mesoporosity. In addition to these morphology and texture studies, it clearly appears from viscosity measurements of the initial co-suspensions that PVP and chitin nanorods are strongly interacting favoring the high orientation of the nanorods through electrospinning. These electrospun porous silica fibers are functionalized easily by incorporating the needed precursors in the initial co-suspensions. The introduction of a monomeric $Ti^{4+}$ precursor leads to isolated and tetrahedral Ti units, distributed in the calcined porous silica fibers. In that respect, these Ti functionalized fibers have very similar characteristics to the Ti functionalized mesoporous microparticles previously obtained by spray-drying co-suspensions with chitin nanorods and possessing interesting properties for the oxidation of sulfur compounds. Additionally, we present preliminary syntheses using zinc xanthate, a ZnS precursor. Zn is successfully incorporated in the fibers at various concentrations. First essays on carbonization lead to the formation of fibers with nanoparticles and Zn and S contents close to ZnS. These examples show the potential of the approach described here for the formation of porous silica-based fibers with desired functionalities for the envisioned applications (like heterogeneous catalysis or photocatalysis).

## Declaration of Competing Interest

The authors declare that they have no competing interests.


## Acknowledgments

ANR is acknowledged for its specific funding through the HYSIKIT ANR Project (Grant ANR-11-BS08-0005); PHC Rila (Grant 29656VM) and Amadeus (OEAD S&T Cooperation program Amadée (project number FR16/2014)) for funding bilateral meetings, EPHE and CNRS for support.


## Supplementary Material

The supplementary materials file contains information and data about: the chemical composition of the fibers, $^{29}Si$ NMR, optical and electron microscopies, the order parameters for the distributions in angles, Ti and ZnS functionalized fibers.

## References


[1] A. Greiner, J.H. Wendorff, Angew. Chem. Int. Ed., 46 (2007) 5670-5703.

[2] J. Xue, T. Wu, Y. Dai, Y. Xia, Chem. Rev., 119 (2019) 5298-5415.

[3] S. Ramakrishna, K. Fujihara, W.-E. Teo, T. Yong, Z. Ma, R. Ramaseshan, Mater. Today, 9 (2006) 40-50.

[4] X. Lu, C. Wang, Y. Wei, Small, 5 (2009) 2349-2370.

[5] J. Lee, Y.L. Deng, Macromol Res., 20 (2012) 76-83.

[6] M.K. Liu, Y.F. Du, Y.E. Miao, Q.W. Ding, S.X. He, W.W. Tjiu, J.S. Pan, T.X. Liu, Nanoscale, 7 (2015) 1037-1046.

[7] C.Y. Xu, R. Inai, M. Kotaki, S. Ramakrishna, Biomaterials, 25 (2004) 877-886.

[8] Z.K. Tan, X.K. Gao, T. Liu, Y.K. Yang, J.C. Zhong, C.Y. Tong, Y.J. Tan, Mater. Sci. Eng. C, 81 (2017) 407-415.

[9] Y.T. Kim, V.K. Haftel, S. Kumar, R.V. Bellamkonda, Biomaterials, 29 (2008) 3117-3127.

[10] L. Yao, N. O'Brien, A. Windebank, A. Pandit, J. Biomed. Mater. Res. B, 90b (2009) 483-491.

[11] M. Richard-Lacroix, C. Pellerin, Macromolecules, 46 (2013) 9473-9493.

[12] J. Yao, C.W.M. Bastiaansen, T. Peijs, Fibers, 2 (2014) 158-187.

[13] D. Papkov, N. Delpouve, L. Delbreilh, S. Araujo, T. Stockdale, S. Mamedov, K. Maleckis, Y. Zou, M.N. Andalib, E. Dargent, V.P. Dravid, M.V. Holt, C. Pellerin, Y.A. Dzenis, ACS Nano, 13 (2019) 4893-4927.

[14] M.V. Kakade, S. Givens, K. Gardner, K.H. Lee, D.B. Chase, J.F. Rabolt, J. Am. Chem. Soc., 129 (2007) 2777-2782.

[15] C.L. Zhang, S.H. Yu, Chem. Soc. Rev., 43 (2014) 4423-4448.

[16] R. Sen, B. Zhao, D. Perea, M.E. Itkis, H. Hu, J. Love, E. Bekyarova, R.C. Haddon, Nano Lett., 4 (2004) 459-464.

[17] A. Šutka, M. Järvekülg, A. Šutka, I. Heinmaa, U. Mäeorg, K. Smits, M. Timusk, Polym. Composites, 39 (2016) 2461-2468.

[18] M. Bashouti, W. Salalha, M. Brumer, E. Zussman, E. Lifshitz, ChemPhysChem, 7 (2006) 102-106.

[19] C.S. Reddy, A. Zak, E. Zussman, J. Mater. Chem., 21 (2011) 16086-16093.

[20] K.E. Roskov, K.A. Kozek, W.-C. Wu, R.K. Chhetri, A.L. Oldenburg, R.J. Spontak, J.B. Tracy, Langmuir, (2011) 13965-13969.

[21] P. Wang, L. Zhang, Y.N. Xia, L.M. Tong, X. Xu, Y.B. Ying, Nano Lett., 12 (2012) 3145-3150.

[22] C.L. Zhang, K.P. Lv, N.Y. Hu, L. Yu, X.F. Ren, S.L. Liu, S.H. Yu, Small, 8 (2012) 2936-2940.

[23] J. Qin, Z.-L. Wen, S. Li, Z.-M. Zhou, J.-J. Hao, D. Wu, H.-C. Liu, W. Chen, B. Xu, D. Wang, R. Chen, K. Wang, X.-W. Sun, Chin. J. Liq. Cryst. Displays, 33 (2018) 262-270.

[24] Y. Dror, W. Salalha, R.L. Khalfin, Y. Cohen, A.L. Yarin, E. Zussman, Langmuir, 19 (2003) 7012-7020.

[25] D. Yang, B. Lu, Y. Zhao, X. Jiang, Adv. Mater., (2007) 3702-3706.

[26] Y.M. Wang, M. Li, J.H. Rong, G.T. Nie, J. Qiao, H.Y. Wang, D.Y. Wu, Z.H. Su, Z.W. Niu, Y. Huang, Colloid Polym. Sci., 291 (2013) 1541-1546.

[27] J. Di, Y. Zhao, J. Yu, J. Mater. Chem., 21 (2011) 8511-8520.

[28] S.F. Anis, A. Khalil, Saepurahman, G. Singaravel, R. Hashaikeh, Microporous Mesoporous Mater., 236 (2016) 176-192.

[29] C. Huang, N.L. Thomas, Polym. Rev., (2019).

[30] Z. Li, J.T. Zhang, Y.M. Chen, J. Li, X.W. Lou, Nat. Commun., 6, (2015) 8850.
[31] C.S. Niu, J.S. Meng, X.P. Wang, C.H. Han, M.Y. Yan, K.N. Zhao, X.M. Xu, W.H. Ren, Y.L. Zhao, L. Xu, Q.J. Zhang, D.Y. Zhao, L.Q. Mai, Nat Commun, 6 (2015) 7042.
[32] Y.M. Sun, R.B. Sills, X.L. Hu, Z.W. Seh, X. Xiao, H.H. Xui, W. Luo, H.Y. Jin, Y. Xin, T.Q. Li, Z.L. Zhang, J. Zhou, W. Cai, Y.H. Huang, Y. Cui, Nano Lett., 15 (2015) 3899-3906.
[33] D. Li, Y. Xia, Nano Lett., 3 (2003) 555-560.
[34] C.J. Brinker, Y. Lu, A. Sellinger, H. Fan, Adv. Mater., 11 (1999) 579-585.
[35] S. Madhugiri, B. Sun, P.G. Smirniotis, J.P. Ferraris, K.J. BalkusJr., Microporous Mesoporous Mater., 69 (2004) 77-83.
[36] S. Zhan, D. Chen, X. Jiao, C. Tao, J. Phys. Chem. B, 110 (2006) 11199-11204.
[37] W. Zhang, R. Zhu, L. Ke, X. Liu, B. Liu, S. Ramakrishna, Small, 6 (2010) 2176-2182.
[38] S.K. Choi, S. Kim, S.K. Lim, H. Park, J. Phys. Chem. C, 114 (2010) 16475-16480.
[39] M. Kim, Y. Kim, K.M. Lee, S.Y. Jeong, E. Lee, S.H. Baeck, S.E. Shim, Carbon, 99 (2016) 607-618.
[40] Z.H. Zhang, B.F. Bai, L. Zeng, L. Wei, T.S. Zhao, Energy Technol., 7 (2019) 1900488.
[41] M.A. Sadeghi, M. Aganou, M. Kok, M. Aghighi, G. Merle, J. Barralet, J. Gostick, J. Electrochem. Soc., 166 (2019) A2121-A2130.
[42] M.D.R. Kok, R. Jervis, T.G. Trantet, M.A. Sadeghi, D.J.L. Brett, P.R. Shearing, J.T. Gostick, Chem. Eng. Sci., 196 (2019) 104-115.
[43] S. Madhugiri, W. Zhou, J.P. Ferraris, K.J. Balkus Jr., Microporous Mesoporous Mater., 63 (2003) 75-84.
[44] Y. Zhao, H. Wang, X. Lu, X. Li, Y. Yang, C. Wang, Mater. Lett., 62 (2008) 143-146.
[45] Y.-N. Wu, F. Li, Y. Wu, W. Jia, P. Hannam, J. Qiao, G. Li, Colloid Polym. Sci., 289 (2011) 1253-1260.
[46] S. Kim, H. Park, H. Choi, Microporous Mesoporous Mater., 2019 (2019) 23-31.
[47] J.D. Schiffman, C.L. Schauer, Polym Rev, 48 (2008) 317-352.
[48] A. Razzaz, S. Ghorban, L. Hosayni, M. Irani, M. Aliabadi, J. Taiwan Inst. Chem. Eng., 58 (2016) 333-343.
[49] T.D. Nguyen, K.E. Shopsowitz, M.J. MacLachlan, Chem. Eur. J., 19 (2013) 15148-15154.
[50] S. Matsumura, S. Kajiyama, T. Nishimura, T. Kato, Small, 11 (2015) 5127-5133.
[51] Y. Yamamoto, T. Nishimura, T. Saito, T. Kato, Polym. J., 42 (2010) 583-586.
[52] D. Qu, J.N. Zhang, G. Chu, H.J. Jiang, C.F. Wu, Y. Xu, J. Mater. Chem. C, 4 (2016) 1764-1768.
[53] J. Xu, T.D. Nguyen, K. Xie, W.Y. Hamad, M.J. MacLachlan, Nanoscale, 7 (2015) 13215-13223.
[54] M. Schlesinger, W.Y. Hamad, M.J. MacLachlan, Soft Matter, 11 (2015) 4686-4694.
[55] A. Lukach, H. Therien-Aubin, A. Querejeta-Fernandez, N. Pitch, G. Chauve, M. Methot, J. Bouchard, E. Kumacheva, Langmuir, 31 (2015) 5033-5041.
[56] G. Chu, X.S. Wang, H. Yin, Y. Shi, H.J. Jiang, T.R. Chen, J.X. Gao, D. Qu, Y. Xu, D.J. Ding, ACS Appl. Mater. Inter., 7 (2015) 21797-21806.
[57] G. Chu, X.S. Wang, T.R. Chen, W. Xu, Y. Wang, H.W. Song, Y. Xu, J. Mater. Chem. C, 3 (2015) 3384-3390.
[58] T.D. Nguyen, W.Y. Hamad, M.J. MacLachlan, Adv. Funct. Mater., 24 (2014) 777-783.
[59] K.E. Shopsowitz, J.A. Kelly, W.Y. Hamad, M.J. MacLachlan, Adv. Funct. Mater, 24 (2014) 327-338.
[60] A. Ivanova, D. Fattakhova-Rohlfing, B.E. Kayaalp, J. Rathousky, T. Bein, J. Am. Chem. Soc., 136 (2014) 5930-5937.

[61] J.A. Kelly, A.M. Shukaliak, C.C.Y. Cheung, K.E. Shopsowitz, W.Y. Hamad, M.J. MacLachlan, Angew. Chem. Int. Ed., 52 (2013) 8912-8916.
[62] K.E. Shopsowitz, A. Stahl, W.Y. Hamad, M.J. MacLachlan, Angew. Chem. Int. Ed., 51 (2012) 6886-6890.
[63] K.E. Shopsowitz, W.Y. Hamad, M.J. MacLachlan, J. Am. Chem. Soc., 134 (2012) 867-870.
[64] H. Qi, K.E. Shopsowitz, W.Y. Hamad, M.J. MacLachlan, J. Am. Chem. Soc., 133 (2011) 3728-3731.
[65] K.E. Shopsowitz, H. Qi, W.Y. Hamad, M.J. MacLachlan, Nature, 468 (2010) 422-425.
[66] B. Alonso, E. Belamie, Angew. Chem. Int. Ed., 49 (2010) 8201-8204.
[67] L. Cardoso, T. Cacciaguerra, P. Gaveau, L. Heux, E. Belamie, B. Alonso, New J. Chem., 41 (2017) 6014-6024.
[68] G. Smolyak, S. Pruvost, L. Cardoso, B. Alonso, E. Belamie, J. Duchet-Rumeau, Carbohydrate Polym., 166 (2017) 139-145.
[69] L. Metselaar, I. Dozov, K. Antonova, E. Belamie, P. Davidson, J.M. Yeomans, A. Doostmohammadi, Phys. Rev. E, 96 (2017) 022706.
[70] M.Y. Boltoeva, I. Dozov, P. Davidson, K. Antonova, L. Cardoso, B. Alonso, E. Belamie, Langmuir, 29 (2013) 8208-8212.
[71] A. Sachse, V. Hulea, K.L. Kostov, N. Marcotte, M.Y. Boltoeva, E. Belamie, B. Alonso, Chem. Commun., 48 (2012) 10648-10650.
[72] A. Sachse, V. Hulea, K.L. Kostov, E. Belamie, B. Alonso, Catal. Sci. Technol., 5 (2015) 415-427.
[73] E. Belamie, P. Davidson, M.M. Giraud-Guille, J. Phys. Chem. B, 108 (2004) 14991-15000.
[74] J.F. Revol, R.H. Marchessault, Int. J. Biol. Macromol., 15 (1993) 329-335.
[75] C.J. Brinker, G.W. Scherer, Sol-Gel Science. The physics and chemistry of Sol-Gel processing, Academic Press, San Diego, 1990.
[76] A.H. Kibbe, Handbook of Pharmaceutical Excipitients, Ed. R.C. Rowe, P.J. Sheskey, M.E. Quinn, sixth ed., The Pharmaceutical Press and the American Pharmacists Association, 2009.
[77] A. Fischereder, A. Schenk, T. Rath, W. Haas, S. Delbos, C. Gougaud, N. Naghavi, A. Pateter, R. Saf, D. Schenk, M. Edler, K. Bohnemann, A. Reichmann, B. Chernev, F. Hofer, G. Trimmel, Monatsh. Chem., 144 (2013) 273-283.
[78] D. Massiot, F. Fayon, M. Capron, I. King, S. Le Calve, B. Alonso, J.O. Durand, B. Bujoli, Z.H. Gan, G. Hoatson, Magn. Reson. Chem., 40 (2002) 70-76.
[79] *Dmfit* downloaded from: https://nmr.cemhti.cnrs-orleans.fr/dmfit/ (last accessed March 21 2022).
[80] J. Schindelin, I. Arganda-Carreras, E. Frise, V. Kaynig, M. Longair, T. Pietzsch, S. Preibisch, C. Rueden, S. Saalfeld, B. Schmid, J.Y. Tinevez, D.J. White, V. Hartenstein, K. Eliceiri, P. Tomancak, A. Cardona, Nat. Methods, 9 (2012) 676-682.
[81] S. Brunauer, P.H. Emmett, E. Teller, J. Am. Chem. Soc., 60 (1938) 309-319.
[82] J.C.P. Broekhoff, J.H. de Boer, J. Catal., 10 (1968) 377-390.
[83] A. Galarneau, D. Desplantier, R. Dutartre, F. DiRenzo, Microporous Mesoporous Mater., 27 (1999) 297-308.
[84] J.H. de Boer, B.C. Lippens, B.G.Linsen, J.C.P. Broekhoff, A. van den Heuvel, T.J. Osinga, J. Colloid Interface Sci., 21 (1966) 405-414.
[85] G. Jura, W.D. Harkins, J. Chem. Phys., 11 (1943) 430-431.

[86] M. Thommes, K. Kaneko, A.V. Neimark, J.P. Olivier, F. Rodriguez-Reinoso, J. Rouquerol, K.S.W. Sing, Pure Appl. Chem., 87 (2015) 1051-1069.
[87] E. Belamie, M.Y. Boltoeva, K. Yang, T. Cacciaguerra, B. Alonso, J. Mater. Chem., 21 (2011) 16997-17006.
[88] S. Hudson, D.A. Tanner, W. Redington, E. Magner, K. Hodnett, S. Nakahara, Phys. Chem. Chem. Phys., 8 (2006) 3467-3474.
[89] M. Klingstedt, K. Miyasaka, K. Kimura, D. Gu, Y. Wan, D. Zhaod, O. Terasaki, J. Mater. Chem., 21 (2011) 13664-13671.
[90] C.P. Lafrance, A. Nabet, R.E. Prud'homme, M. Pezolet, Can. J. Chem., 73 (1995) 1497-1505.
[91] J.H. Park, Y.L. Joo, Soft Matter, 10 (2014) 3494-3505.
[92] L. Vachoud, S.C.d. Carvalho, A. Bayart, N. Armand, L. Cardoso, B. Alonso, E. Belamie, Colloids Surf. A, 558 (2018) 470-478.
[93] E. Prouzet, C. Boissière, S.S. Kim, T.J. Pinnavaia, Microporous Mesoporous Mater., 119 (2009) 9-17.
[94] E. Vakalopoulou, C. Buchmaier, A. Pein, R. Saf, R.C. Fischer, A. Torvisco, F. Warchomicka, T. Rath, G. Trimmel, Dalton Trans., 49 (2020) 14564-14575